Huang *et al.*
BMC Complementary Medicine and Therapies (2025) 25:75
https://doi.org/10.1186/s12906-025-04751-y

BMC Complementary Medicine and Therapies

RESEARCH Open Access

UHPLC-Q Exactive-Orbitrap-MS and network pharmacology analyses to investigate the mechanism by which Danggui-Shaoyao-San affects 27-OHC-induced cell damage in SH-SY5Y/C6 coculture

Yi Huang[1†], Yingying Zhai[2†], Di Zhao[1], Mingan Wu[1], Qi Shen[1], Wei Zhao[1], Qi Wang[1], Limei Yao[3*] and Weirong Li[1*]

Abstract

Background Danggui-Shaoyao-San (DSS) is a classic Chinese medicine formula that has been extensively studied for its efficacy in treating Alzheimer's disease (AD). However, its mechanism of action is still unclear.

Methods In this study, UHPLC-Q Exactive-Orbitrap-MS was used to analyze and identify the compounds in DSS. Network pharmacology was used to analyze the common targets of drug-containing serum chemistries and AD, as well as the AD pathways in which drug-containing serum chemistries may be involved. The 27-OHC-induced SH-SY5Y/C6 coculture cell injury model was used to explore the mechanism of action of DSS in the treatment of AD.

Results UHPLC-Q Exactive-Orbitrap-MS analysis identified 73 chemical constituents in DSS aqueous extract and 39 compounds in drug-containing serum. According to network pharmacology analysis, DSS and AD share 181 common targets, with interleukin-6 (IL-6) and tumor necrosis factor (TNF) being the main effective targets. Furthermore, DSS may treat AD through the modulation of lipid metabolism-related pathways and the interleukin-17 (IL-17) signaling pathway. 27-hydroxycholesterol acid (27-OHC) significantly reduced the viability of SH-SY5Y cells and C6 cells in vitro, while DSS administration upregulated the expression of cytochrome P450 46A1 (CYP46A1) and cytochrome P450 7B1 (CYP7B1) enzymes and reduced cholesterol levels in SH-SY5Y cells. Additionally, DSS decreased reactive oxygen species (ROS) levels and increased glutathione (GSH) levels in coculture systems. DSS downregulated the expression of IL-17 in 27-OHC-injured SH-SY5Y cells and downregulated the expression of TNF-α, IL-6 and transforming growth factor-β1 (TGF-β1) in 27-OHC-injured C6 cells.

Conclusion This study revealed the effective components, targets and mechanisms of DSS in the treatment of AD, highlighting the significant potential of DSS in treating this disease.

†Yi Huang and Yingying Zhai contributed equally to this work and should be considered co-first authors.

*Correspondence:
Limei Yao
yaolm2000@126.com
Weirong Li
liwr@gzucm.edu.cn
Full list of author information is available at the end of the article

Keywords Danggui-Shaoyao-San, Alzheimer's disease, Lipid metabolism, Network pharmacology, 27-hydroxycholesterol acid, Neuroinflammation

Introduction

Alzheimer's disease (AD) is the most common form of dementia, and the associated pathological changes include abnormal amyloid deposition, accumulation of phosphorylated tau protein [1–3], and neuronal degeneration [4, 5]. The World Health Organization estimates that by 2050, there will be 2.1 billion people aged 60 and older, with 426 million aged 80 and older [6]. Age is a major risk factor for AD. The World Health Organization (WHO) projects that as global populations continue to age, the number of individuals diagnosed with dementia will increase to 139 million by 2050 and that the cost of treatment will reach more than US $2.8 trillion by 2030 [4], posing a serious challenge to global public health and social development. Although there have been significant advances in the diagnosis and treatment of AD in recent years, a cure for this disease has not yet been found.

The Danggui-Shaoyao-San (DSS) used in this study was obtained from Zhang Zhongjing's *Jingui Yaolue*. Clinically, DSS can improve the symptoms of patients with AD and vascular dementia (VD) [7]. DSS can reduce the content and deposition of amyloid beta (Aβ) in the brains of mice [8, 9], reduce amyloidosis [10], and improve spatial memory and learning ability in mice. In addition, DSS can regulate neuronal apoptosis induced by oxidative stress and $A\beta_{1\text{-}42}$ [11–13]. DSS has been shown to improve central cholinergic nervous system dysfunction, increase acetylcholine (Ach) levels and protect neurons [14, 15]. We discovered that DSS can enhance cognitive function in APP/PS1 double transgenic AD mice by regulating the metabolism of docosahexaenoic acid (DHA) in the brain. Additionally, it can regulate blood lipid levels to improve cognitive impairment induced by a high-cholesterol diet in mice [16]. Although several studies have reported the therapeutic effects of DSS on AD, the specific molecular mechanisms through which DSS affects AD have not been determined.

High-performance liquid chromatography combined with mass spectrometry (UHPLC/MS) is a widely used tool for qualitative and quantitative analysis in all stages of drug development [17]. It is highly effective at detecting and identifying drug components and metabolites [18]. Network pharmacology analysis is a multidisciplinary research method characterized by its integrity, systematization, and comprehensiveness [19, 20]. It has been widely used in the study of traditional Chinese medicine compounds. In this study, the chemical components of DSS were analyzed qualitatively and quantitatively using UHPLC/MS, and the drug target network of the chemical components of DSS drug-containing serum was analyzed by network pharmacology to target AD. To provide more experimental basis for clinical drug treatment of AD, we further conducted experiments to investigate the role and mechanism of DSS against AD.

Materials and methods

Materials and reagents

The six herbs of DSS were purchased from Kangmei Pharmaceutical Co., Ltd. (Puning, China). All the herbs were identified by Zhao Wei, an associate researcher at the Science and Technology Innovation Center of Guangzhou University of Chinese Medicine, and all the samples were stored at the Science and Technology Innovation Centre of Guangzhou University of Chinese Medicine. Mass spectrometry-grade acetonitrile and mass spectrometry-grade methanol were purchased from Thermo Fisher Scientific Co., Ltd. (Waltham, MA, USA). All other reagents were of analytical grade. Total cholesterol, ROS and GSH assay kits were purchased from Nanjing Jiancheng Bioengineering Research Institute Co., Ltd. (Nanjing, China). Real-time quantitative PCR reagents were purchased from Sangon Biotechnology (Shanghai, China). The rat TNF-α ELISA kit, rat IL-6 ELISA kit, rat IL-17 ELISA kit, rat TGF-β1 ELISA kit, human TGF-β1 ELISA kit, human IL-10 ELISA kit and human IL-17 ELISA kit were purchased from CUSABIO (Wuhan, China).

Animals

Forty SPF-grade male Sprague–Dawley rats weighing 180–220 g were purchased from the Guangdong Medical Laboratory Animal Center (Certificate No. SCXK Guangdong, 44,007,200,103,712) and kept in an SPF-grade laboratory of the Sanyuanli Animal Experiment Center, Guangzhou University of Chinese Medicine. The temperature of the room was kept at 25 ± 2 ℃, while the humidity was maintained between 55 and 65%. All rats were provided food and water ad libitum. Before the experiment, the rats were adaptively fed for 1 week and randomly divided into a blank serum group and a DSS-containing serum group, with 20 rats in each group. This study was approved by the Ethics Committee of Guangzhou University of Chinese Medicine and was conducted in accordance with the committee's guidelines (Approval

No. 20210508001). All animal experiments reported in accordance with ARRIVE guidelines (https://arriveguidelines.org).

Sample preparation

According to the DSS recipe (Table 1) to weigh 130 g herbs, and soaked in 10 volumes of water, then heating refluxed for 1 h. The filtrate was collected, then the herbs added 8 volumes of water and was heating refluxed for 1 h again. Finally, the collected filtrate was mixed with the filtrate of the first time. The filtrate was concentrated to 2 g (crude drug)/mL by rotary steaming at 50 °C, lyophilized and stored for later use. The lyophilized DSS powder (10 mg) was weighed and diluted in water to prepare a sample solution with a mass concentration of 100 ng/ml.

Rats in the DSS-containing serum group were given 2 g/mL DSS solution by gavage, and rats in the blank serum group were given the same volume of normal saline by gavage once a day for 7 days. The animals were fasted for 12 h before the last dose. Rats were anesthetized with 2% isoflurane (EZVET, Beijing, China) 1 h after the last gavage, anesthesia was maintained with 2% isoflurane, and blood samples were collected from the abdominal aorta. Rats were euthanized by decapitation under anesthesia. After isolation, the serum was inactivated in a water bath at 56 °C for 30 min and filtered through a 0.22 μm filter membrane. Three volumes of acetonitrile were added to the serum, which was then mixed and centrifuged at 12,000 rpm for 15 min at 4 °C. The supernatant was removed, dried under nitrogen, and the samples were redissolved in 100 μL of methanol. The fivefold enriched samples were obtained by centrifuging again for 15 min. The supernatant was collected for injection and analyzed in UHPLC-Q Exactive-Orbitrap-MS.

UHPLC-Q Exactive Orbitrap-MS analysis

Chromatography was performed on an ultrahigh-performance liquid chromatograph (Vanquish Duo UHPLC system) (Thermo Fisher Scientific, Waltham, MA, USA). A Waters ACQUITY UPLC BEH C18 column (2.1 mm × 100 mm, 1.8 μM) was used with 0.1% formic acid aqueous (A)-0.1% formic acid-acetonitrile (B) as the mobile phase. The gradient elution sequence was as follows: 0–5 min with 2–5% B, 5–35 min with 5–40% B, 35–50 min with 40–100% B, 50–53 min with 100% B, 53–58 min with 100–2% B, and 58–60 min with 2% B. The column temperature was maintained at 35 °C, and the volume flow rate was set at 0.3 mL/min. The injection volume of the DSS extract solution was 2 μL, and the injection volume of the serum sample solution was 5 μL.

Mass spectrometry was performed using a Thermo Scientific Q Exactive-Orbitrap high-resolution mass spectrometer (Thermo Fisher Scientific, Waltham, MA, USA). The data were collected and analyzed on an Xcalibur system workstation (Thermo, USA). Mass spectrometry was performed using an electron spray ionization (ESI) source in positive and negative ionization modes, and the data were collected from m/z 80–1200. The operating conditions of the ESI source were as follows: capillary temperature, positive and negative ion mode spray voltages, sheath gas flow rate, and auxiliary gas flow rate were 350 ℃, 3800 V, 3200 V, 35 arb, and 15 arb, respectively.

Table 1 DSS recipe

Components	Dosage
Angelica sinensis (Oliv.) Diels	60 g
Paeonia lactiflora Pall	320 g
Ligusticum chuanxiong Hort	160 g
Poria cocos (Schw.) Wolf	80 g
Atractylodes macrocephala Koidz	80 g
Alisma orientale(Sam.) Juzep	160 g

Network pharmacology analysis

The active ingredients of DSS target collection

The pubchem database (https://pubchem.ncbi.nlm.nih.gov) was used to obtain the active ingredients and their Simplified Molecular Input Line Entry System (SMILES), and then the SMILES numbers were imported into the structural similarity prediction target database, Swiss Target Prediction, to predict the effective targets.

Identification of AD-associated targets

The GeneCards database (http://www.genecards.org) and the online Mendelian Inheritance in Man (https://omim.org/) database were used, and the search terms 'Alzheimer's disease' and 'AD' were used. Online Venny software (https://bioinfogp.cnb.cic.es/tools/venny/) was used to identify intersections between active ingredient targets and disease targets [21].

Construction of the DSS active ingredient-target disease networks

A compound, target, disease, and drug name network was constructed using Cytoscape 3.9.2 software. The nodes represent compounds, targets, diseases, and drug names, and the edges represent interactions between nodes. The network revealed the interactions of the active ingredients of DSS with anti-AD targets.

PPI network construction and analysis

The intersections of the drug targets and AD-related targets were analyzed using the STRING platform (https://

www.string-db.org) for protein–protein interaction analysis [22]. A protein–protein interaction (PPI) network was constructed, and the top 9 potential targets of DSS against AD were identified.

GO and KEGG enrichment analysis

The bioinformatics open source software Bioconductor (http: //www.bioconductor.org/) was utilized to perform Gene Ontology (GO) and Kyoto Encyclopedia of Genes and Genomes (KEGG) pathway analyses [23]. These analyses were also conducted to identify potential targets of DSS for the treatment of AD. KEGG pathway analysis revealed signaling pathways that elucidate the mechanism of the anti-AD effect.

In vitro *protocol*

Cell culture

Human neuroblastoma cells (SH-SY5Y) and rat astrocytoma (C6) cells were purchased from the Ek-Biosciences Cell Bank (Shanghai, China). SH-SY5Y and C6 cells were cocultured on inserted Petri dishes. SH-SY5Y cells were inoculated into 6-well plates at a density of 0.9×10^7 cells/mL with 2.6 mL per well, while C6 cells were inoculated into microporous membranes (pore size of 0.4 μM) of inserted dishes at a density of 0.75×10^6 cells/mL with 1.5 mL per well. After inoculation, the cells were incubated at 37 °C in a 5% CO_2 incubator for 4 h. Subsequently, the cells were seeded into a 6-well plate and incubated for 20 h for further experimentation.

Establishment of the 27-OHC model

To prepare a 2 mmol/L reserve solution, 10 mg of 27-hydroxycholesterol (27-OHC) (Shanghai Yuanye Bio-Technology Co., Ltd., Shanghai, China) was dissolved in 12.42 mL of anhydrous ethanol and mixed with the culture solution before use. A previous study was performed to investigate the effects of various concentrations of 27-OHC on the activity of SH-SY5Y and C6 cells. Ultimately, the optimal concentration of 27-OHC was determined to be 10 μM, which resulted in a 50–60% survival rate for both cell lines.

Determination of total cholesterol, ROS, and GSH content

SH-SY5Y/C6 cells were cocultured. After culture, SH-SY5Y cells were collected and resuspended according to the instructions of the total cholesterol, ROS and GSH kits. The total cholesterol data are expressed as mmol/g protein; the ROS data are expressed as fluorescence intensity/mg protein; and the GSH data are expressed as μmol/g protein.

Evaluation of the IL-6, TNF-α, IL-17, TGF-β, and IL-10 concentrations

The concentrations of IL-6, TNF-α, IL-17, TGF-β, and IL-10 were measured using an ELISA kit. The absorbance values of each standard and sample were measured at 450 nm using an enzyme labeling instrument. The concentration of each standard and absorbance value were used to fit a standard curve in Curve Expert software (Thermo Fisher Scientific, Waltham, MA, USA). The concentrations of the samples were determined by subtracting the absorbance value of the S0 wells from the OD values of the sample wells.

Quantitative real-time polymerase chain reaction (qRT–PCR)

After coculturing the SH-SY5Y and C6 cells, the culture mixture was removed, trypsin was added to collect the SH-SY5Y cells, and RNA was extracted using 1 mL of TRIzol. The RNA was then analyzed for quantity and purity using a spectrophotometer (Imolen, Germany). Subsequently, reverse transcription was performed to obtain cDNA using an RNA reversal kit, and the RNA was analyzed using a real-time fluorescence quantitative PCR instrument (Bio-Rad, USA). The primer sequences are presented in Table 2.

Statistical analyses

The data are expressed as the means ± standard deviations ($\overline{X}\pm S$) and were compared using an independent samples t test or one-way ANOVA. A post hoc test was performed using the LSD method. Differences between means were considered significant at $P<0.05$. The data were analyzed using IBM SPSS Statistics 22 software (IBM Corp., Armonk, NY, USA). Graphs were generated using GraphPad Prism 8.0.

Table 2 Primer sequence

Gene	Primer sequence (5′-3′)
CYP46A1	F: TGCTTTTGGAAAAAGGATGAGG
	R: AACAGGTCCATACTTCTTAGCC
CYP7B1	F: CAGCAGTGCGTGACGAAATTGAC
	R: TGTTCTCTGGTGAGGTGGATGGG
AP-N	F: GAAGGACAGCCAGTATGAGATG
	R: GGATAAGCGTGATGTTGAACTC
AP-A	F: CAATGCCTTACRCTGTGATTCG
	R: CTAATGACTTTGGGGTTACTGC

Results

DSS component analysis

DSS UHPLC-Q Exactive-Orbitrap-MS chromatograms

According to the chromatographic conditions, DSS-treated rat serum samples (Fig. 1A, B), chromatograms of the DSS compound samples (Fig. 1C, D), and blank rat serum samples (Fig. 1E, F) were collected.

Analysis of DSS aqueous extract chemical composition

The exact mass-to-charge ratios (m/z) of the compounds were obtained by Q Exactive-Orbitrap-MS, and the secondary fragment ions of this mass were obtained by secondary mass spectrometry. Cholesterol MSP (https://old.Triglyceride msp-e.com/triglyceridemsp.php), cholesterol MID (https://ngdc.cncb.ac.cn/databasecommons/database/id/437), PubChem (https://pubchem.ncbi.nlm.nih.gov/) and other databases were used to query the literature within the databases of China Knowledge (https://www.cnki.net/) to establish the six Chinese herbs in the DSS compound formula. The information in the database included chemical composition, molecular formula, secondary fragmentation information, etc., and the structures of the relevant compounds were analyzed qualitatively. Finally, the chemical components of the DSS compound were identified, and a total of 73 chemical components were obtained. The specific results are shown in Table 3.

Analysis of the chemical constituents of DSS-containing serum

Based on the accurate relative molecular mass of the compounds, the fragmentation information of each compound and the relevant literature and database information, a total of 39 chemical components were identified in the DSS-containing serum. The DSS blood entry-related components mainly included organic acids, terpenoids, phenols, sesquiterpenoids, and sesquiterpene compounds. In addition, we examined blank serum samples and identified proline, adenine, pyroglutamic acid, tyrosine, and 7-hydroxycoumarin not only as being derived from DSS but also as endogenous components inherent to the serum. The specific results of the chemical composition of the DSS-containing serum and the identification of the blank serum are shown in Table 3.

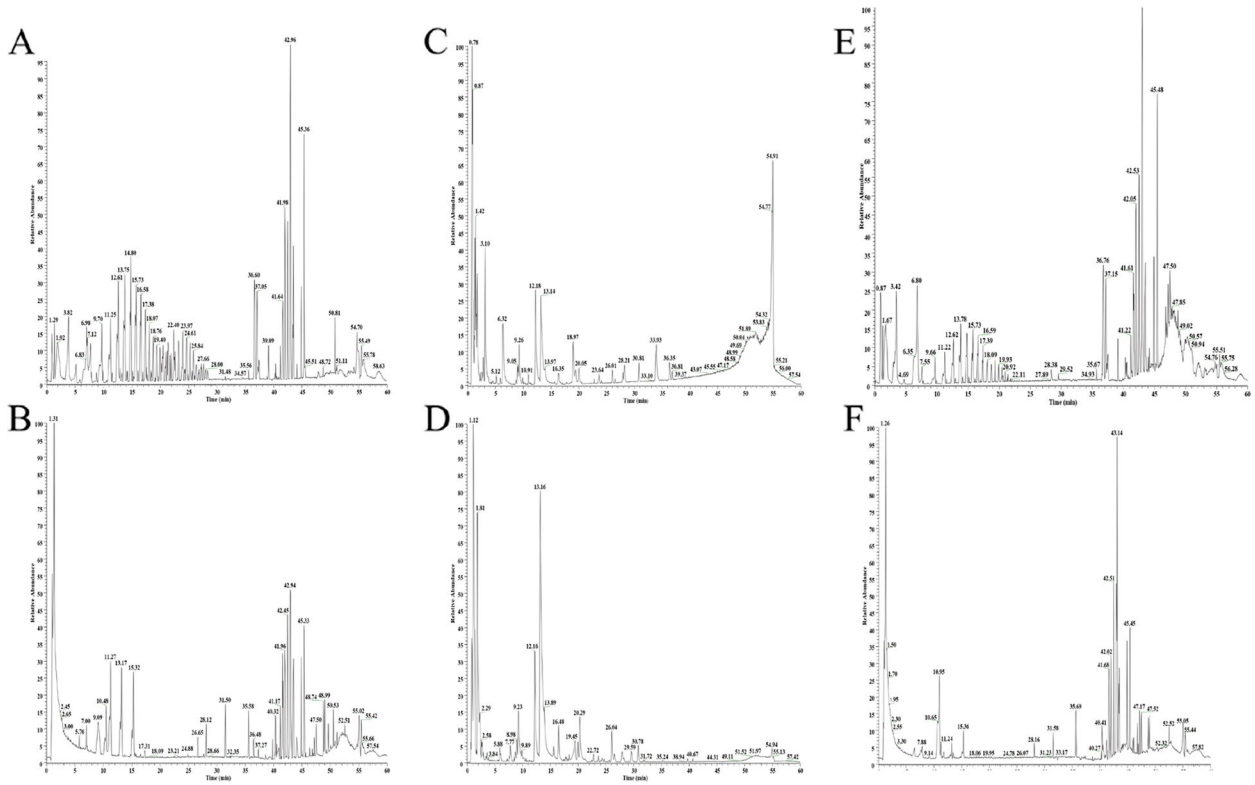

Fig. 1 **A**, **B** Positive (**A**) and negative (**B**) peak ion flow chromatograms of UHPLC-Q Exactive-Orbitrap-MS of DSS rat drug-containing serum samples. **C**, **D** Positive (**C**) and negative (**D**) peak ion flow chromatograms of UHPLC-Q Exactive-Orbitrap-MS of DSS compound samples. **E**, **F** Positive (**E**) and negative (**F**) peak ion flow chromatograms of the positive (**E**) and negative (**F**) key peaks of the blank rat serum sample UHPLC-Q Exactive-Orbitrap-MS

Table 3 Chemical composition information of DSS compound

Peak No	tR(min)	Pattern	Compound of DSS aqueous extract	compound of DSS-containing serum	Compound of blank serum	Molecular Formula	Value of measurement(m/z)	Theoretical value(m/z)	ppm	MS/MS	Type of component	Sources and references
1	0.70	$[M+H]^+$	arginine	arginine		$C_6H_{14}N_4O_2$	175.1189	175.1190	-0.57	175.1195, 158.0930, 116.0709	Organic acids	Danggui [24]
2	0.79	$[M+H]^+$	Choline choline	Choline choline		$C_5H_{13}NO$	104.1069	104.1070	-0.96	104.1073, 87.0443	Organic base	Danggui [24]
3	0.85	$[M-H]^-$	sucrose			$C_{12}H_{22}O_{11}$	341.1098	341.1089	2.64	341.1103, 119.0356, 89.0247, 71.0140, 59.0138	Glycosides	Shaoyao [25]
4	0.92	$[M+H]^+$	adenine	adenine	adenine	$C_5H_5N_5$	136.0617	136.0618	-0.73	136.0623, 119.0355	Purines	Chuanxiong [26, 27]
5	0.92	$[M+H]^+$	proline	proline	proline	$C_5H_9NO_2$	116.0705	116.0706	-0.86	116.0709, 70.0655	Organic acids	Danggui [24]
6	1.01	$[M+H]^+$	Pyroglutamic acid	Pyroglutamic acid	Pyroglutamic acid	$C_5H_7NO_3$	130.0501	130.0499	1.54	130.0504, 102.0553, 84.0447	Organic acids	Danggui [24]
7	1.09	$[M+H]^+$	5-hydroxym-ethylfurfural	5-hydroxym-ethylfurfural		$C_6H_6O_3$	127.0387	127.0390	-2.36	127.0394, 109.0288, 97.0288, 81.0338, 55.0183	furans	Baizhu [28]
8	1.09	$[M+H]^+$	Pyrogallol	Pyrogallol		$C_6H_6O_3$	127.0387	127.0390	-2.36	127.0394, 110.0433, 109.0288	Phenols	Shaoyao [29]
9	1.10	$[M+H]^+$	5-hydroxym-ethyl-2-furan formaldehyde	5-hydroxym-ethyl-2-furan formaldehyde		$C_6H_6O_3$	127.0387	127.0390	-2.36	127.0394, 109.0288	furans	Danggui [24]
10	1.12	$[M-H]^-$	Citric acid	Citric acid		$C_6H_8O_7$	191.0203	191.0197	3.14	191.0205, 111.0093, 87.0090, 85.0298, 57.0345	Organic acids	Shaoyao [25]
11	1.42	$[M+H]^+$	Tyrosine kinase	Tyrosine kinase	Tyrosine kinase	$C_9H_{11}NO_3$	182.0811	182.0812	-0.55	182.0811, 165.0552	Organic acids	Danggui [24]
12	1.42	$[M+H]^+$	Adenosine			$C_{10}H_{13}N_5O_4$	268.1028	268.1040	-4.48	268.1022, 136.0623	Pyranes	Danggui [24]
13	1.81	$[M-H]^-$	Gallic acid	Gallic acid		$C_7H_6O_5$	169.0149	169.0142	4.14	169.0150, 125.0250, 107.0144	Polyphenols	Shaoyao [29]

Table 3 (continued)

Peak No	tR(min)	Pattern	Compound of DSS aqueous extract	compound of DSS-containing serum	Compound of blank serum	Molecular Formula	Value of measurement(m/z)	Theoretical value(m/z)	ppm	MS/MS	Type of component	Sources and references
14	2.14	$[M-H]^-$	Desbenzoyl paeoniflorin	Desbenzoyl paeoniflorin		$C_{16}H_{24}O_{10}$	375.1307	375.1297	2.67	345.1200, 195.0668, 151.0771	Terpenoids	Shaoyao [25]
15	2.58	$[M-H]^-$	Paeonone-1-O-β-D-Glucoside	Paeonone-1-O-β-D-Glucoside		$C_{16}H_{24}O_9$	359.1355	359.1348	1.95	359.1349, 179.0720, 85.0297	Glycosides	Shaoyao [25]
16	3.06	$[M+H]^+$	Cinnamic acid			$C_9H_8O_2$	149.0596	149.0597	-0.67	149.0238, 131.0495, 103.0545	Cinnamic acids	Chuanxiong [26, 27]
17	3.26	$[M+H]^+$	phenylalanine	phenylalanine		$C_9H_{11}NO_2$	166.0862	166.0863	-0.60	166.0867, 149.0603, 120.0811, 103.0545	Organic acids	Danggui [24]
18	3.64	$[M-H]^-$	Diglucosyl gallate			$C_{19}H_{26}O_{15}$	493.1196	493.1199	-0.61	493.1193 313.0567, 169.0150, 151.0044	Glycosides	Shaoyao [25]
19	5.52	$[M-H]^-$	Methyl gallate	Methyl gallate		$C_8H_8O_5$	183.0306	183.0299	3.82	183.0307, 139.0408, 124.0173	Benzoic acids	Shaoyao [29]
20	5.97	$[M+H]^+$	Salicylic acid	Salicylic acid		$C_7H_6O_3$	139.0391	139.0390	0.72	139.0399, 121.0294, 116.9726	Benzoic acids	Shaoyao [29]
	6.15	$[M-H]^-$					137.0252	137.0244	5.84	137.0251, 119.0146, 93.0350	Benzoic acids	Shaoyao [29]
21	7.12	$[M+H]^+$	Ligustrazine	Ligustrazine		$C_8H_{12}N_2$	137.1079	137.1073	4.38	137.0967, 122.0843, 109.1016, 81.0702	Pyrazines	Chuanxiong [26, 27]
22	8.43	$[M+H]^+$	Oxidized paeoniflorin			$C_{23}H_{28}O_{12}$	497.1650	497.1654	-0.80	497.2051, 197.0816, 121.0288	Terpenoids	Shaoyao [30]
23	8.69	$[M+H]^+$	Catechin	Catechin		$C_{15}H_{14}O_6$	291.0850	291.0863	-4.47	291.0881, 139.0395, 123.0445	Phenols	Shaoyao [29]

Table 3 (continued)

Peak No	tR(min)	Pattern	Compound of DSS aqueous extract	compound of DSS-containing serum	Compound of blank serum	Molecular Formula	Value of measurement(m/z)	Theoretical value(m/z)	ppm	MS/MS	Type of component	Sources and references
24	8.91	$[M+H]^+$	Chlorogenic acid			$C_{16}H_{18}O_9$	355.1006	355.1024	-5.07	163.0396, 145.0290, 117.0339, 89.0389	Polyphenols	Baizhu [28]
25	8.95	$[M+H]^+$	7-hydroxycoumarin	7-hydroxycoumarin	7-hydroxycoumarin	$C_9H_6O_3$	163.0387	163.0390	-1.84	163.0396, 145.0290, 135.0446, 117.0339, 107.0495, 89.0389	Coumarins	Baizhu [31]
26	9.19	$[M-H]^-$	Caffeic acid			$C_9H_8O_4$	179.0365	179.0350	8.38	179.0357, 135.0459, 107.0509	Benzoic acids	Chuanxiong [26, 27]
27	9.23	$[M-H]^-$	Vanilloid acid	Vanilloid acid		$C_8H_8O_4$	167.0357	167.0350	4.19	167.0358, 123.0458	Benzoic acids	Chuanxiong [26, 27]
28	11.82	$[M+H]^+$	Paeonol	Paeonol		$C_9H_{10}O_3$	167.0703	167.0703	0.00	167.0706, 125.0601, 121.0652	Phenols	Shaoyao [29]
29	12.18	$[M+H]^+$	Paeonolactone B			$C_{10}H_{12}O_4$	197.0808	197.0808	0.00	197.0814, 151.0758, 133.0652	Terpenoids	Shaoyao [29]
30	13.14	$[M+H]^+$	Paeoniflorin			$C_{23}H_{26}O_{10}$	463.1586	463.1599	-2.81	463.2151, 151.0758, 105.0701	Terpenoids	Shaoyao [30]
31	13.16	$[M-H]^-$	Paeonidin E	Paeonidin E		$C_{24}H_{30}O_{13}$	525.1602	525.1614	-2.29	327.1094, 165.0565, 121.0301	Terpenoids	Shaoyao [25]
32	13.16	$[M-H]^-$	Paeonifloride	Paeonifloride		$C_{23}H_{28}O_{11}$	479.1559	479.1559	0.00	327.1098, 165.0565, 121.0301	Terpenoids	Shaoyao [29]
33	13.90	$[M-H]^-$	Ferulic acid	Ferulic acid		$C_{10}H_{10}O_4$	193.0512	193.0506	3.11	193.0513, 178.0278, 149.0615, 134.0380	Cinnamic acids	Chuanxiong [26, 27] Danggui [24]
34	13.97	$[M+H]^+$	Dimethyl phthalate	Dimethyl phthalate		$C_{10}H_{10}O_4$	195.0651	195.0652	-0.51	195.1158, 121.0652	Benzoic acids	Shaoyao [29]
35	14.91	$[M-H]^-$	Ellagic acid			$C_{14}H_6O_8$	300.9997	300.9990	2.33	300.9994, 229.0147	Polyphenols	Shaoyao [25]

Table 3 (continued)

Peak No	tR(min)	Pattern	Compound of DSS aqueous extract	compound of DSS-containing serum	Compound of blank serum	Molecular Formula	Value of measurement(m/z)	Theoretical value(m/z)	ppm	MS/MS	Type of component	Sources and references
36	15.46	$[M-H]^-$	Sinapic acid			$C_{11}H_{12}O_5$	223.0617	223.0612	2.24	223.0618, 179.0721	Fatty acids	Chuanxiong [26, 27]
37	16.35	$[M+H]^+$	The K/G isomer of Ligusticolide			$C_{12}H_{16}O_3$	209.1169	209.1172	-1.43	192.1110, 164.1158, 136.1208	Phenols	Danggui [24, 32]
38	16.48	$[M-H]^-$	Gallic paeoniflorin			$C_{30}H_{32}O_{15}$	631.1722	631.1668	8.56	613.1651, 491.1199, 313.0570	Terpenoids	Shaoyao [29]
39	17.77	$[M+H]^+$	Dihydroxybutylphthalide isomers			$C_{12}H_{14}O_4$	223.0960	223.0965	-2.24	223.0606, 205.0862, 181.0861	Phenols	Danggui [24, 32]
40	19.03	$[M+H]^+$	Ligusticolide F			$C_{12}H_{14}O_3$	207.1013	207.1016	-1.45	207.1021, 189.0918, 179.1071, 161.0967, 147.0807, 133.0653, 119.0860, 105.0702	Phenols	Danggui [24, 32]
41	19.03	$[M+H]^+$	4-hydroxy-3-butylphthalide			$C_{12}H_{14}O_3$	207.1013	207.1016	-1.45	207.1021, 189.0918, 161.0968, 133.0654	Phenols	Chuanxiong [26, 27]
42	19.41	$[M-H]^-$	Paeoniflorin	Paeoniflorin		$C_{23}H_{28}O_{11}$	479.1559	479.1559	0.00	327.1078, 121.0301	Terpenoids	Shaoyao [29]
43	20.05	$[M+H]^+$	Atractylodes ketone			$C_{15}H_{20}O$	217.1581	217.1587	-2.76	217.1591, 199.1489, 157.1019, 131.0861, 129.0703, 119.0860	Sesquiterpenes	Baizhu [33, 34]
44	20.32	$[M+H]^+$	Poria lactone I			$C_{15}H_{20}O_2$	233.1528	233.1536	-3.43	233.1537, 215.1433, 79.0546	Sesquiterpenes	Baizhu [28]

Table 3 (continued)

Peak No	tR(min)	Pattern	Compound of DSS aqueous extract	compound of DSS-containing serum	Compound of blank serum	Molecular Formula	Value of measurement(m/z)	Theoretical value(m/z)	ppm	MS/MS	Type of component	Sources and references
45	22.22	$[M+H]^+$	Atractylodes lactone III	Atractylodes lactone III		$C_{15}H_{20}O_3$	249.1474	249.1485	-4.42	249.1489, 231.1373, 161.1329, 119.0859, 91.0545, 79.0546	Sesquiterpenes	Baizhu [28]
46	23.54	$[M+H]^+$	Atractylodes lactoneVI			$C_{15}H_{22}$	203.1791	203.1794	-1.48	203.1800, 161.1331, 147.1174, 133.1017, 119.0859, 105.0702, 79.0543	Sesquiterpenes	Baizhu [28]
47	24.28	$[M+H]^+$	Prickly ash toxin			$C_{12}H_8O_4$	217.0490	217.0495	-2.30	217.0498, 202.0269	Coumarins	Chuanxiong [26, 27]
48	24.30	$[M-H]^-$	Ligusticolide D	Ligusticolide D		$C_{12}H_{14}O_4$	221.0824	221.0819	2.26	221.0824, 177.0928	Phenols	Chuanxiong [26, 27]
49	24.30	$[M-H]^-$	4, 7-dihydroxy-3-butylphthalide	4, 7-dihydroxy-3-butylphthalide		$C_{12}H_{14}O_4$	221.0824	221.0819	2.26	221.0824, 177.0928	Phenols	Chuanxiong [26, 27]
50	26.53	$[M+H]^+$	Benzoyl paeoniflorin			$C_{30}H_{32}O_{12}$	585.1950	585.1967	-2.91	249.0760, 197.0818, 105.0339	Terpenoids	Shaoyao [25]
51	27.90	$[M+H]^+$	Butylphthalide	Butylphthalide		$C_{12}H_{12}O_2$	189.0909	189.0910	-0.53	189.0917, 171.0810, 143.0861, 128.0625, 91.0546	Phenols	Chuanxiong [26, 27]
52	27.95	$[M+H]^+$	Ligustractone	Ligustractone		$C_{12}H_{12}O_2$	189.0910	189.0910	0.00	189.0917, 171.0810, 161.0968	Phenols	Danggui [24]
53	28.16	$[M+H]^+$	3-n-butylphthalide	3-n-butylphthalide		$C_{12}H_{14}O_2$	191.1064	191.1067	-1.57	191.1075, 117.0703, 91.0546	Phenols	Chuanxiong [26, 27]
54	28.16	$[M+H]^+$	Z-ligustilide	Z-ligustilide		$C_{12}H_{14}O_2$	191.1064	191.1067	-1.57	191.1075, 145.1018, 117.0703, 105.0702, 91.0546	Phenols	Chuanxiong [26, 27] Danggui [24]

Table 3 (continued)

Peak No	tR(min)	Pattern	Compound of DSS aqueous extract	compound of DSS-containing serum	Compound of blank serum	Molecular Formula	Value of measurement(m/z)	Theoretical value(m/z)	ppm	MS/MS	Type of component	Sources and references
55	28.19	$[M-H]^-$	Ligusticolide K	Ligusticolide K		$C_{12}H_{16}O_3$	207.1033	207.1027	2.90	207.1033, 163.1136	Phenols	Chuanxiong [26, 27]
56	28.19	$[M-H]^-$	Ligusticolide G	Ligusticolide G		$C_{12}H_{16}O_3$	207.1033	207.1027	2.90	207.1033, 163.1136	Phenols	Chuanxiong [26, 27]
57	28.47	$[M+H]^+$	Alisene epoxide	Alisene epoxide		$C_{15}H_{24}O$	221.1895	221.1900	-2.26	221.1901, 203.1799, 161.1332, 147.1174, 133.1017, 95.0858	Sesquiterpenes	Zexie [35]
58	30.81	$[M+H]^+$	alismanol M			$C_{30}H_{48}O_6$	505.3524	505.3524	0.00	487.3443, 415.2843, 397.2732	Terpenoids	Zexie [35]
59	31.98	$[M-H]^-$	Ligusticolide B			$C_{12}H_{12}O_3$	203.0720	203.0714	2.95	203.0719, 174.0329, 160.0173	Phenols	Chuanxiong [26, 27]
60	31.98	$[M-H]^-$	Ligusticolide C			$C_{12}H_{12}O_3$	203.0720	203.0714	2.95	203.0719, 174.0329, 160.0173	Phenols	Chuanxiong [26, 27]
61	33.72	$[M+H]^+$	Alismatol C			$C_{30}H_{46}O_5$	487.3415	487.3418	-0.62	469.3318, 451.3225, 353.2473	Terpenoids	Zexie [35]
62	33.84	$[M-H]^-$	Ligusticolide A	Ligusticolide A		$C_{12}H_{16}O_2$	193.1224	193.1223	0.52	119.0496, 91.0546	Phenols	Chuanxiong [26, 27]
63	34.49	$[M+H]^+$	alisol L			$C_{30}H_{44}O_4$	469.3302	469.3312	-2.13	469.2864, 451.3210, 353.2469	Terpenoids	Zexie [35]
64	35.02	$[M+H]^+$	Atractylodes lactone II	Atractylodes lactone II		$C_{15}H_{18}O_2$	231.1381	231.1380	0.43	231.1381, 213.1280, 185.1333, 157.1018	Sesquiterpenes	Baizhu [28]
65	35.27	$[M+H]^+$	24-deacetyl alisol O			$C_{30}H_{46}O_4$	471.3462	471.3469	-1.49	453.3363, 435.3271, 381.2786, 363.26982	Terpenoids	Zexie [35]
66	36.66	$[M+H]^+$	16-oxo-11-anhydro-alisol A			$C_{30}H_{46}O_5$	487.3415	487.3418	-0.62	469.3344, 451.3220, 397.2733	Terpenoids	Zexie [35]

Table 3 (continued)

Peak No	tR(min)	Pattern	Compound of DSS aqueous extract	compound of DSS-containing serum	Compound of blank serum	Molecular Formula	Value of measurement(m/z)	Theoretical value(m/z)	ppm	MS/MS	Type of component	Sources and references
67	38.00	$[M+H]^+$	New serpentol-actone	New serpentol-actone		$C_{12}H_{18}O_2$	195.1382	195.1380	1.02	195.1388, 177.1282, 149.1331	Sesquiterpenes	Chuanxiong [26, 27]
68	38.66	$[M+H]^+$	alismanol O			$C_{30}H_{46}O_6$	503.3374	503.3367	1.39	467.3150, 413.2690	Terpenoids	Zexie [35]
69	38.97	$[M+H]^+$	23-acetylalis-berol C			$C_{32}H_{48}O_6$	529.3530	529.3524	1.13	529.3546, 469.3322, 451.3217, 433.3107, 415.2850	Terpenoids	Zexie [35]
70	39.44	$[M+H]^+$	Sessile Costus lactone			$C_{15}H_{20}O_2$	233.1537	233.1536	0.43	215.1436, 187.1488, 131.0863, 105.0703	Sesquiterpenes	Baizhu [33, 34]
71	40.64	$[M+H]^+$	Ivy sapogenin			$C_{30}H_{48}O_4$	473.3617	473.3625	-1.69	147.1174, 121.1016	Terpenoids	Shaoyao [29]
72	40.64	$[M+H]^+$	Alismatol B			$C_{30}H_{48}O_4$	473.3617	473.3625	-1.69	383.2931, 365.2828, 339.2675	Terpenoids	Zexie [35]
73	44.24	$[M+H]^+$	Pachymic acid			$C_{33}H_{52}O_5$	529.3842	529.3888	-8.69	529.3546, 511.3421, 451.3217	Terpenoids	Fuling [36]

Active ingredients and potential targets of DSS

The TCMSP traditional chinese medicine database revealed 13 valid targets in proline; 12 valid targets in choline, 5-hydroxymethyl-2-furaldehyde, adenine, gallic acid, paeonidin E, paeoniflorin, 7-hydroxycoumarin, ligusticolide K, and butylphthalide; 9 valid targets in arginine; 13 valid targets in 5-hydroxymethylfurfural, ligustrazine, vanillic acid, and paeonol; 31 valid targets in pyrogallol; 15 valid targets in citric acid, pyroglutamic acid, phenylalanine, and ferulic acid; 19 valid targets in tyrosine kinase and 4,7-dihydroxy-3-butylphthalide; 11 valid targets in desbenzoyl paeoniflorin, catechin, and paeonone-1-O-β-D-glucoside; 14 valid targets in dimethyl phthalate, paeonifloride, ligusticolide D, ligustractone; 18 valid targets in methyl gallate; 10 valid targets in salicylic acid and alisene epoxide; 17 valid targets in ligusticolide G and atractylodes lactone III; 20 valid targets in 3-n-butylphthalide; and 26 valid targets in z-ligustilide. A total of 11,501 AD target genes were obtained from the GeneCards database, and 385 AD target genes were obtained from the OMIM database. After taking the top 1000 genes according to the GeneCards correlation scores and the set of all target genes in the OMIM database and removing duplicates, disease targets for AD were obtained. The targets for DSS and AD were entered into Venny, and a total of 181 shared targets were obtained (Fig. 2A).

Protein–protein interaction networks

Using the StringPlatform, a PPI network consisting of 55 nodes and 265 edges was constructed based on the 181 common targets for potential DSS-related anti-AD targets (Fig. 2B). By analyzing the topological parameters of the network, AKT serine/threonine kinase 1 (AKT1), jun proto-oncogene (JUN), heat shock protein 90 alpha family class a member 1 gene (HSP90AA1), IL-6, TNF, estrogen receptor 1 (ESR1), mitogen-activated protein kinase 1 (MAPK1), interleukin-1 beta (IL1B), epidermal growth factor receptor (EGFR) were found to play important roles in the network.

Active ingredient-target-disease network

Using Cytoscape 3.9.2 software, a network of 253 nodes and 554 edges was constructed between potential therapeutic targets of AD drugs and DSS (Fig. 2C). The built-in network analyzer was used to analyze the degrees of the nodes, in which the degree-valued active ingredients associated with the most DSS-related targets were pyrogallol and z-ligustilide.

GO enrichment and KEGG pathway analysis

The GO enrichment and KEGG pathway analysis results revealed that DSS and AD shared 181 enriched targets. These targets were analyzed based on biological processes, cellular components, and molecular functions. The results were related to "nuclear receptor activity," "ligand-activated transcription factor activity" (Fig. 2D). According to the KEGG pathway analysis, "lipid and atherosclerosis," "AGE-RAGE signaling pathway in diabetic complications," "fluid shear stress and atherosclerosis," and "IL-17 signaling pathway" were the key pathways (Fig. 2E).

Effect of DSS on 27-OHC-induced cell damage in SH-SY5Y/C6 cocultures

Effect of DSS on 27-OHC-induced damage to SH-SY5Y and C6 cell viability

The MTT results showed that DSS administration significantly improved the viability of 27-OHC-injured SH-SY5Y and C6 cells (Fig. 3A, B). These results demonstrate that DSS protects SH-SY5Y and C6 cells by antagonizing the toxic effects of 27-OHC.

Effect of DSS on the cholesterol content of SH-SY5Y cells in the 27-OHC-damaged coculture system

27-OHC caused cellular damage and elevated cholesterol levels in SH-SY5Y cells ($P<0.05$), whereas a decrease in cholesterol content in SH-SY5Y cells was observed after treatment with different doses of DSS (Fig. 3C). As expected, DSS ameliorated the 27-OHC-induced increase in cholesterol.

Effect of DSS on CYP46A1 and CYP7B1 expression in 27-OHC-damaged coculture system-generated SH-SY5Y cells

To investigate the involvement of CYP46A1 and CYP7B1 in regulating cholesterol metabolism, we used PCR to eliminate their mRNA expression. We observed that in the model group, the number of SH-SY5Y cells with CYP46A1 and CYP7B1 mRNA expression decreased ($P<0.001$), the medium-dose DSS treatment significantly elevated the expression of CYP7B1 mRNA ($P<0.001$), and the high-dose DSS treatment significantly increased the expression of CYP46A1 and CYP7B1 mRNA (Fig. 3D, E). These results support a critical effect of DSS in upregulating CYP46A1 and CYP7B1 enzyme expression.

Effect of DSS on oxidative stress in 27-OHC-damaged cocultured cells

The results showed a significant increase in the ROS content in both the SH-SY5Y and C6 cells in the model group ($P<0.001$) (Fig. 4A, C). However, treatment with DSS at low, medium, or high doses resulted in a significant reduction in the ROS concentration in both cell lines ($P<0.001$) (Fig. 4A, C).

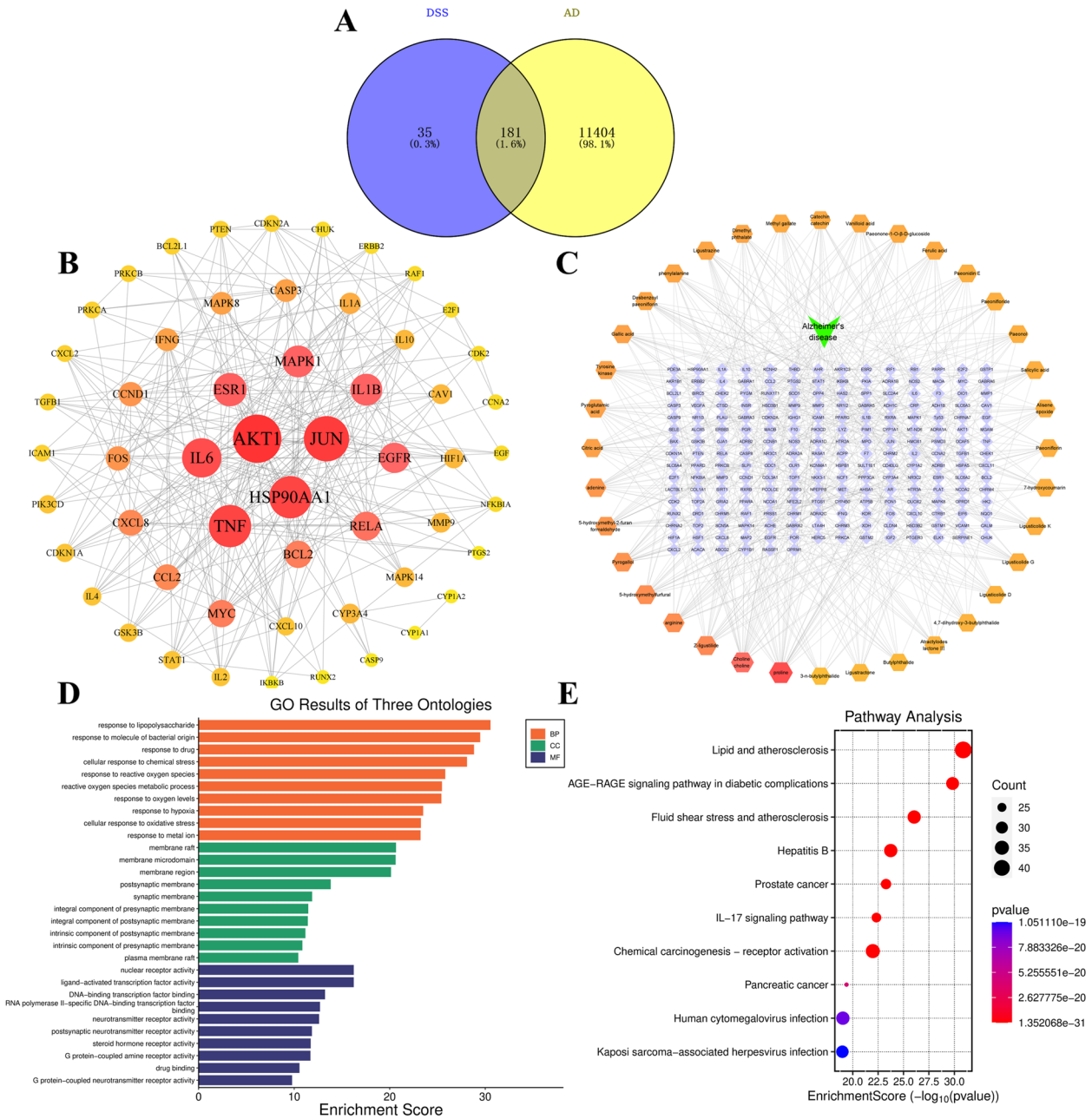

Fig. 2 **A** Drug-disease Venn diagram for DSS and AD. **B** PPI network diagram for DSS against AD. **C** Drug target-AD network plot for DSS. **D** Potential target enrichment analysis for GO analysis of DSS (BP: biological process, CC: cellular component, MF: molecular function). **E** Potential target enrichment analysis for DSS (KEGG analysis)

The model group showed a significant decrease in GSH content in both the SH-SY5Y cells and C6 cells ($P < 0.001$) (Fig. 4B, D). In contrast, the GSH content in the SH-SY5Y cells in the low-, medium-, and high-dose DSS groups significantly increased ($P < 0.001$) (Fig. 4B). The DSS low- and high-dose groups also showed an increase in GSH content in C6 cells ($P < 0.05$) (Fig. 4D). These findings suggest that DSS can increase glutathione levels, reduce ROS levels, and alleviate oxidative stress.

Effect of DSS on inflammatory factor expression in the 27-OHC-injured coculture system

An increase in TNF-α levels ($P < 0.001$) and a decrease ($P < 0.001$) were detected in the model group and DSS medium- and high-dose groups of C6 cells, respectively

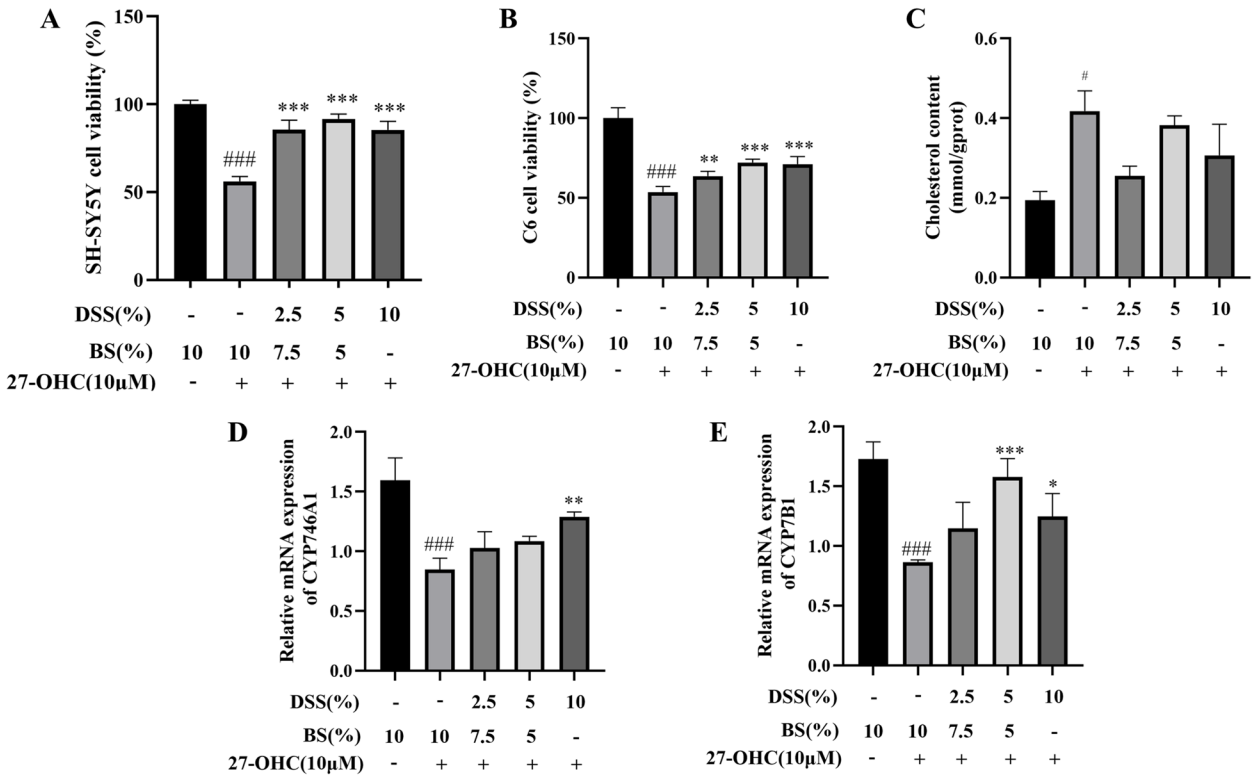

Fig. 3 **A** Effect of DSS on SH-SY5Y cell viability. **B** Effect of DSS on C6 cell viability. **C** Effect of DSS on the cholesterol content of SH-SY5Y cells in the 27-OHC-injured coculture system. **D**, **E** Effects of DSS on CYP46A1 and CYP7B1 mRNA expression in 27-OHC-injured SH-SY5Y cells. DSS(%): the content of DSS-containing serum; BS(%): the content of blank serum. Compared with the control, $^{\#}P<0.05$, $^{\#\#}P<0.01$, and $^{\#\#\#}P<0.001$; compared with the model, $^{*}P<0.05$, $^{**}P<0.01$, and $^{***}P<0.001$. All values are presented as the mean ± standard deviation. $n=3$

(Fig. 4E). The IL-6 concentration increased in the model group ($P<0.05$) and decreased in the DSS low-dose group ($P<0.05$) (Fig. 4F). The TGFβ1 concentration decreased in the model group ($P<0.05$), while the TGFβ1 concentration increased in the middle-dose DSS group ($P<0.01$) (Fig. 4H). There were no significant differences in the IL-17 concentration among the groups (Fig. 4G).

An assay of SH-SY5Y cells revealed that the IL-17 concentration was elevated in the model group ($P<0.001$) and decreased in the low-, medium-, and high-dose DSS groups ($P<0.01$) (Fig. 4I). The IL-10 concentration decreased in the model group ($P<0.01$), while there was no significant change in the IL-10 concentration in the DSS dose groups (Fig. 4K). Moreover, there was no significant change in the TGF-β1 concentration among the groups (Fig. 4J). These results indicate that DSS has some anti-inflammatory effects.

Discussion

Abnormal lipid metabolism is a significant factor in the pathogenesis of AD, as the brain is the most lipid-rich organ [37, 38]. Hypercholesterolemia resulting from lipid dysregulation is a high risk factor for neurodegenerative diseases that can lead to AD-like pathology [39–41]. Research has demonstrated that hypercholesterolemia induced by a high-cholesterol diet can lead to oxidative stress in cells. This can also accelerate the accumulation of Aβ and phosphorylation of tau proteins, increase the level of inflammatory factors, and cause spatial learning and memory deficits, ultimately accelerating the progression of AD [42]. Clinical studies have shown that DSS is effective at treating dyslipidemia [43] and can be used to treat AD [44]. Studies have also demonstrated that DSS can reduce serum cholesterol, triacylglycerol (TG), and low-density lipoprotein cholesterol (LDL-C) levels while increasing high-density lipoprotein cholesterol (HDL-C) levels in rats fed a high-fat diet [45]. In a previous study, we found that DSS can improve cognitive function in APP/PS1 double transgenic AD model mice by regulating docosahexaenoic acid (DHA) metabolism in the brain [16]. However, the mechanism of action of DSS to improve AD by improving lipid metabolism has not been clarified.

In our study, the chemical constituents of DSS were analyzed by UHPLC-Q Exactive-Orbitrap-MS. A total of 73 chemical constituents were identified in DSS aqueous

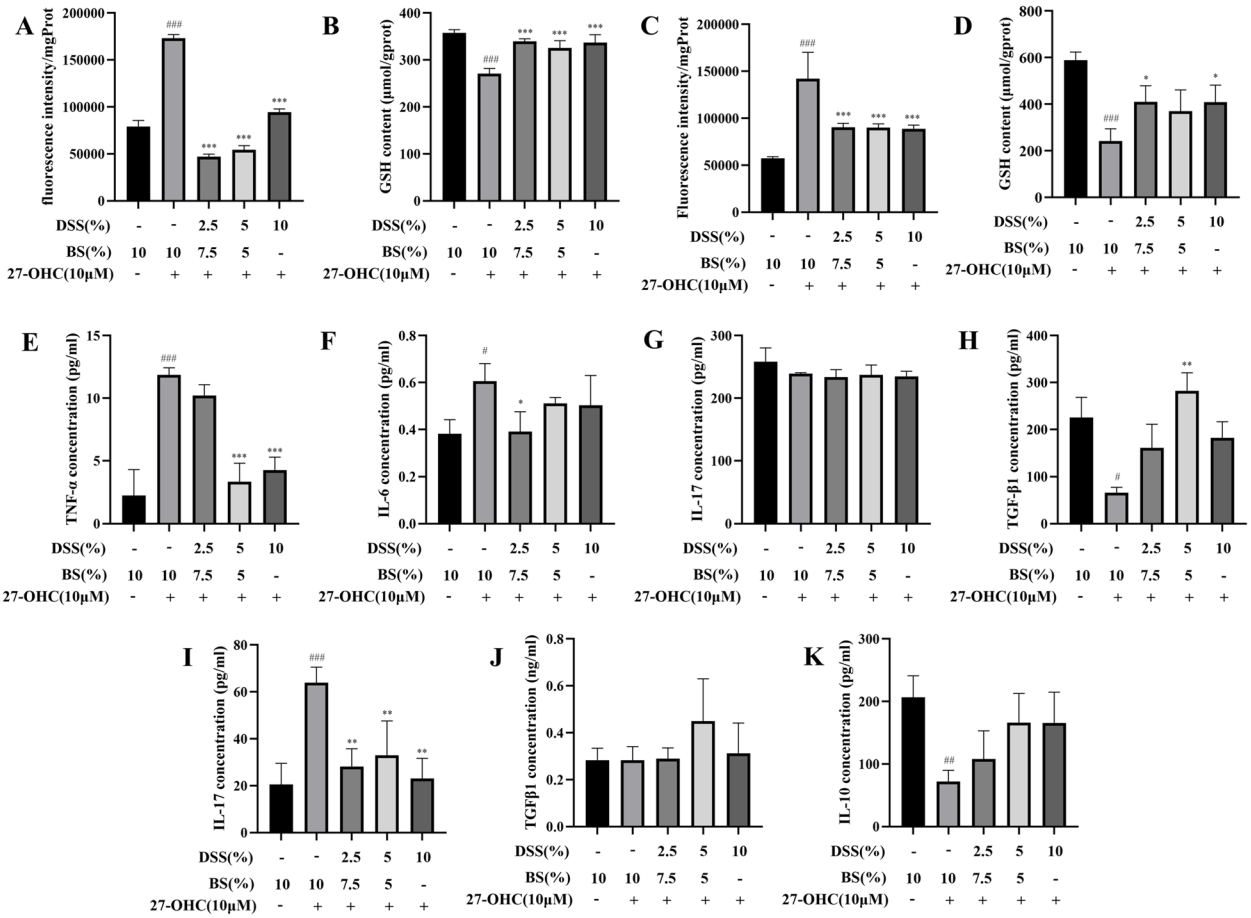

Fig. 4 **A** Effect of DSS on ROS in SH-SY5Y cells. **B** Effect of DSS on the GSH in SH-SY5Y cells. **C** Effect of DSS on ROS in C6 cells. **D** Effect of DSS on the GSH in C6 cells. **E**, **F**, **G**, **H** Effects of DSS on TNF-α, IL-6, IL-17, and TGF-β1 in C6 cells. **I**, **J**, **K** Effects of DSS on IL-17, TGF-β1, and IL-10 in SH-SY5Y cells. DSS(%): the content of DSS-containing serum; BS(%): the content of blank serum. Compared with the control, $^{\#}P<0.05$, $^{\#\#}P<0.01$, and $^{\#\#\#}P<0.001$; compared with the model, $^{*}P<0.05$, $^{**}P<0.01$, and $^{***}P<0.001$. All values are presented as the mean ± standard deviation. $n=3$

extract, and 39 chemical constituents were identified in the DSS drug-containing serum. This study utilized network pharmacology to analyze the chemical components of DSS drug-containing serum. DSS had 181 common targets associated with AD, including IL-6, TNF, IL1B, AKT1, and EGFR, which are closely related to lipid metabolism and inflammation [46–49]. KEGG analysis indicated that DSS has the potential to treat AD by targeting lipid metabolism-related and IL-17 signaling pathway-related pathways. Thus, our conducted in vitro experiments to further explore the mechanism of action of DSS to improve AD.

Hypercholesterolemia is one of the high risk factors for neurodegenerative diseases, and hypercholesterolemia causes AD-like pathology [39–41]. Cholesterol is a crucial lipid in the brain. Although peripheral cholesterol cannot directly penetrate the blood–brain barrier, it can enter the brain by synthesizing 27-OHC via cytochrome P450 27A1 (CYP27A1). The investigation of AD pathology in rabbits on a high cholesterol diet and high levels of 27-OHC showed a significant decrease in leptin expression levels, along with an increase in the hyperphosphorylated content of Aβ and tau proteins [50]. There are also studies that show that mice injected with 27-OHC had increased brain deposition of Aβ and amyloid A-serum amyloid A (SAA) precursors and exhibited poorer cognitive function in the water maze [51]. Investigation of the relationship between 27-OHC and cholesterol homeostasis revealed that ApoE epsilon4 transgenic mice injected with 27-OHC had reduced cognitive function and upregulated levels of cholesterol-transporting proteins in the brain, such as apolipoprotein E (ApoE), low-density lipoprotein receptor (LDLR), and LDLR-associated protein 1 (LRP1), which was ameliorated by a 27-OHC synthetase inhibitor [52]. In exploring the toxicity and mechanisms of AD-like pathology induced by 27-OHC, it was found that 27-OHC activated the TGF-β/NF-κB signaling pathway in C6 cells [53], increased the

level of ROS, and decreased the levels of total superoxide dismutase (T-SOD), reduced GSH, and glutathione peroxidase (GSH-PX) [54], which contributed to neuronal inflammatory and oxidative stress damage. Therefore, to explore the molecular mechanisms of DSS against AD, we next used a 27-OHC-induced SH-SY5Y/C6 co-culture cell injury model to further explore the mechanisms of DSS against AD.

27-OHC is present in large amounts in the blood and can enter the brain from the periphery and is a major cause of memory impairment induced by a high cholesterol diet [55]. This process can lead to disrupted lipid metabolism, neuronal damage, and neuronal apoptosis, ultimately resulting in cognitive dysfunction [56, 57]. One pathway of cholesterol metabolism in the brain involves its conversion to 24-hydroxycholesterol acid (24-OHC) through CYP46A1, which then enters the peripheral circulation [58]. Autopsy results have shown a significant decrease in 24-OHC levels and a significant increase in 27-OHC levels during the late stages of AD [59], with an increased 24-OHC/27-OHC ratio. In experiments comparing normal and knockout CYP46A1 mice on a high cholesterol diet, researchers found that the expression levels of activity-regulated cytoskeletal-associated proteins were reduced in normal mice. However, the expression levels of cytoskeletal-associated proteins were not significantly altered in knockout CYP46A1 mice due to the reduced conversion to cholesterol, which protects the brain tissue [56, 60]. 24-OHC and 27-OHC are considered biomarkers for diagnosing AD [61]. Changes in the levels of the enzymes CYP46A1 and CYP7B1 can reflect lipid metabolism [62]. The results of this study showed that DSS administration upregulated the expression of CYP46A1 and CYP7B1 mRNA in 27-OHC-injured SH-SY5Y cells and reduced the cholesterol content in SH-SY5Y cells. This may be one of the mechanisms by which DSS can treat AD by regulating lipid metabolism as shown in network pharmacology results.

Lipids are the main components of cell membranes, and when oxidative stress occurs during lipid peroxidation, the structural integrity of cell membranes is disrupted [63]. Moreover, highly reactive lipid peroxides can accelerate the formation of ROS [64], generating oxidized metabolites that are harmful to brain tissue and impair cognitive function [65–67]. Thus, an imbalance between oxidation and antioxidants affects cognitive function. ROS are primarily produced by microglia [68]. Oxidative stress caused by excessive ROS and reactive nitrogen species (RNS) [69] can lead to direct damage to lipids and cognitive dysfunction [70]. One way to treat oxidative stress caused by ROS is to increase the amount of free radical scavengers and antioxidants [68]. GSH is a crucial component of the body's nonenzymatic antioxidant system, and cognitive dysfunction is often accompanied by a loss of GSH in the brain [71]. The results of this study indicated that DSS can decrease ROS levels and increase GSH expression in SH-SY5Y and C6 cells in a 27-OHC-induced injury model. These findings suggest that DSS can improve the level of oxidative stress in both neuronal and glial cells.

Neuroinflammation is an inflammatory response in the central nervous system caused by glial cell activation and is inextricably linked to the development of oxidative stress [72]. Glial cell activation produces many proinflammatory cytokines, such as interleukins (IL-1β, IL-6, and IL-18), TNF, and chemokines (CCL1, CCL5, and CXCL1) [73], which result in synaptic dysfunction, neuronal death, and the inhibition of long-term potentiation, promoting cognitive impairment [74, 75]. Activated microglia not only release proinflammatory signaling molecules and neurotoxins but also form a vicious cycle of proinflammatory signaling molecules, which continuously enhances neuroinflammation and promotes the development of AD [73, 76]. Through network pharmacology analysis, the results of this study identified numerous targets related to inflammatory factors that could be potential anti-AD targets. In vitro, DSS administration downregulated the expression of the inflammatory factor IL-17 in 27-OHC-injured SH-SY5Y cells and the inflammatory factors TNF-α, IL-6, and TGF-β1 in 27-OHC-injured C6 cells. These findings suggest that DSS has anti-inflammatory effects on both neuronal and glial cells.

Although our study yielded encouraging results, importantly, the composition of DSS is complex, and we are still unable to determine which components of DSS play protective roles against 27-OHC injury in the coculture cell system.

To summarize this study, UHPLC-Q Exactive-Orbitrap-MS analysis was used to identify the chemical composition of DSS, and 73 compounds in the DSS aqueous extract and 39 compounds in the DSS drug-containing serum were preliminarily identified. Network pharmacological analysis was used in this study, and 181 common targets were found between DSS and AD, of which IL-6, TNF, IL1B, AKT1, and EGFR were the main effective targets. Additionally, DSS might treat AD through lipid metabolism and IL-17 signaling pathways. Additionally, this study used a SH-SY5Y/C6 coculture system model of 27-OHC-induced injury to examine both neuronal and glial cells. In vitro experiments revealed that DSS administration upregulated the expression of CYP46A1 and CYP7B1, reduced cholesterol levels in neuronal cells, decreased ROS levels in neuronal and glial cells, increased the expression of GSH, and decreased the expression of inflammatory factors.

These effects ameliorated neuronal cell injury induced by 27-OHC cholesterol.

To further investigate the potential regulatory mechanisms of DSS on the lipid and atherosclerosis pathway, we will hypothesise that impairment of 27-OHC may result in abnormal lipid metabolism, which in turn may contribute to the development of AD. We will then test the indicators of apolipoprotein E (ApoE), low-density lipoprotein receptor (LDLR) and low-density lipoprotein receptor-related protein 1 (LRP1) expression, with a view to gaining insights into the pharmacological effects of DSS in the treatment of AD.

Conclusions

In conclusion, our study utilized UHPLC-Q Exactive-Orbitrap-MS to identify a total of 73 chemical constituents in DSS aqueous extract, and 39 chemical constituents in the DSS drug-containing serum. Through network pharmacology analysis, DSS-containing serum contains targets relevant to AD therapy and has the potential to treat AD by targeting lipid metabolism-related pathways. What's more, further in vitro experiments have shown that DSS can mitigate 27-OHC-induced neuronal cell damage by regulating cholesterol metabolism, reducing oxidative stress and inflammation. These findings suggest that DSS may be a potential clinical treatment for AD caused by abnormal lipid metabolism.

Abbreviations

AD	Alzheimer's disease
Aβ	Amyloid β-protein
CASP3	Cysteinyl aspartate specific proteinase-3
CAT	Catalase
CYP 46A1	Cytochrome P450 46A1
CYP7B1	Cytochrome P450 7B1
DSS	Danggui-Shaoyao-San
GSH	Glutathione
ESI	Electron spray ionization
GO	Gene Ontology
IL-6	Interleukin-6
IL-17	Interleukin-17
IL-10	Interleukin-10
KEGG	Kyoto Encyclopedia of Genes and Genomes
27-OHC	27-Hydroxycholesterol acid
24-OHC	24-Hydroxycholesterol acid
ROS	Reactive oxygen species
PPARG	Peroxisome proliferator activated receptor gamma
PPI	Protein–protein interaction
PTGS2	Prostaglandin-endoperoxide synthase 2
TGF-β1	Transforming growth factor-β1
TNF	Tumor necrosis factor
TNF-α	Tumor necrosis factor-alpha

Supplementary Information

The online version contains supplementary material available at https://doi.org/10.1186/s12906-025-04751-y.

Supplementary Material 1.

Acknowledgements

We thank Sangon for providing primer design services as well as synthetic primers.

Authors' contributions

Y.H. drafted the manuscript. Y.Z. contributed to the design of this study. D.Z. contributed in manuscript preparation. M.W contributed in visualization of experimental results. Q.S. assisted with experiments. W.Z., L.Y. and Q.W. contributed in revising the manuscript and funding acquisition. W.L. revised and edited the manuscript. All the authors have read and approved this version of the manuscript.

Funding

This work was supported by the National Natural Science Foundation of China [grant numbers 82074505, 82374547, 82274616, 81973919]; and Guangdong Basic and Applied Basic Research Foundation [grant numbers 2023A1515011835, 2022A1515220121].

Data availability

The datasets used and analyzed during the present study are available from the corresponding author upon reasonable request.

Declarations

Ethics approval and consent to participate

The animal study was carried out in compliance with the ARRIVE guidelines. All animal procedures were approved and conducted according to the Animal Experimentation Ethics Committee guidelines, as evidenced by the Ethics Committee of Guangzhou University of Chinese Medicine (Guangzhou, China), with approval No. 20210508001.

Consent for publication

Not applicable.

Competing interests

The authors declare no competing interests.

Author details

[1]Science and Technology Innovation Center, Guangzhou University of Chinese Medicine, Guangzhou, China. [2]School of Pharmacy, Xinyang Agriculture and Forestry University, Henan, China. [3]School of Traditional Chinese Medicine Healthcare, Guangdong Food and Drug Vocational College, Tianhe District, 321 Longdong North Road, Guangzhou 510520, China.

Received: 21 March 2024 Accepted: 7 January 2025
Published online: 24 February 2025

References

1. Grundke-Iqbal I, Iqbal K, Tung YC, Quinlan M, Wisniewski HM, Binder LI. Abnormal phosphorylation of the microtubule-associated protein tau (tau) in Alzheimer cytoskeletal pathology. Proc Natl Acad Sci U S A. 1986;83(13):4913–7.
2. Hardy JA, Higgins GA. Alzheimer's disease: the amyloid cascade hypothesis. Science. 1992;256(5054):184–5.
3. Oddo S, Caccamo A, Shepherd JD, Murphy MP, Golde TE, Kayed R, Metherate R, Mattson MP, Akbari Y, Laferla FM. Triple-transgenic model of Alzheimer's disease with plaques and tangles: intracellular Abeta and synaptic dysfunction. Neuron. 2003;39(3):409–21.
4. Alzheimer's disease facts and figures. Alzheimers Dement. 2023;19(4):1598–695.
5. Price JL, Ko AI, Wade MJ, Tsou SK, Mckeel DW, Morris JC. Neuron number in the entorhinal cortex and CA1 in preclinical Alzheimer disease. Arch Neurol. 2001;58(9):1395–402.
6. Long S, Benoist C, Weidner W. World Alzheimer Report 2023: Reducing dementia risk: never too early, never too late. London, England: Alzheimer's Disease International; 2023.

7. Kim Y, Cho SH. Danggui-Shaoyao-San for dementia: A PRISMA-compliant systematic review and meta-analysis. Medicine (Baltimore). 2020;99(4):e18507.
8. Hu ZY, Liu G, Yuan H, Yang S, Zhou WX, Zhang YX, Qiao SY. Danggui-Shaoyao-San and its active fraction JD-30 improve Abeta-induced spatial recognition deficits in mice. J Ethnopharmacol. 2010;128(2):365–72.
9. Hu ZY, Liu G, Cheng XR, Huang Y, Yang S, Qiao SY, Sun L, Zhou WX, Zhang YX. JD-30, an active fraction extracted from Danggui-Shaoyao-San, decreases beta-amyloid content and deposition, improves LTP reduction and prevents spatial cognition impairment in SAMP8 mice. Exp Gerontol. 2012;47(1):14–22.
10. Yang C, Mo YS, Chen HF, Huang YH, Li SL, Wang H, Huang SQ, Chang X, Du Q, Wang Q. The effects of Danggui-Shaoyao-San on neuronal degeneration and amyloidosis in mouse and its molecular mechanism for the treatment of Alzheimer's disease. J Integr Neurosci. 2021;20(2):255–64.
11. Huang Z, Mao QQ, Zhong XM, Li ZY, Qiu FM, Ip SP. Mechanistic study on the antidepressant-like effect of danggui-shaoyao-san, a chinese herbal formula. Evid Based Complement Alternat Med. 2012;2012:173565.
12. Lan Z, Liu J, Chen L, Fu Q, Luo J, Qu R, Kong L, Ma S. Danggui-Shaoyao-San ameliorates cognition deficits and attenuates oxidative stress-related neuronal apoptosis in d-galactose-induced senescent mice. J Ethnopharmacol. 2012;141(1):386–95.
13. Song Z, Luo D, Wang Y, Zheng Y, Chen P, Xia X, He C, Yu W, Li P, Xiao C, Cheng S. Neuroprotective Effect of Danggui Shaoyao San via the Mitophagy-Apoptosis Pathway in a Rat Model of Alzheimer's Disease. Evid Based Complement Alternat Med. 2021;2021:3995958.
14. Hatip-Al-Khatib I, Hatip FB, Yoshimitsu Y, Iwasaki K, Egashira N, Liu AX, Mishima K, Fujiwara M. Effect of Toki-shakuyaku-san on acetylcholine level and blood flow in dorsal hippocampus of intact and twice-repeated ischemic rats. Phytother Res. 2007;21(3):291–4.
15. Itoh T, Michijiri S, Murai S, Saito H, Nakamura K, Itsukaichi O, Fujiwara H, Ookubo N, Saito H. Regulatory effect of danggui-shaoyao-san on central cholinergic nervous system dysfunction in mice. Am J Chin Med. 1996;24(3–4):205–17.
16. Huang J, Wang X, Xie L, Wu M, Zhao W, Zhang Y, Wang Q, Yao L, Li W. Extract of Danggui-Shaoyao-San ameliorates cognition deficits by regulating DHA metabolism in APP/PS1 mice. J Ethnopharmacol. 2020;253:112673.
17. Beccaria M, Cabooter D. Current developments in LC-MS for pharmaceutical analysis. Analyst. 2020;145(4):1129–57.
18. Tolonen A, Turpeinen M, Pelkonen O. Liquid chromatography–mass spectrometry in in vitro drug metabolite screening. Drug Discov Today. 2009;14(3–4):120–33.
19. Zhao L, Zhang H, Li N, Chen J, Xu H, Wang Y, Liang Q. Network pharmacology, a promising approach to reveal the pharmacology mechanism of Chinese medicine formula. J Ethnopharmacol. 2023;309:116306.
20. Hopkins AL. Network pharmacology: the next paradigm in drug discovery. Nat Chem Biol. 2008;4(11):682–90.
21. Davis AP, Grondin CJ, Johnson RJ, Sciaky D, Wiegers J, Wiegers TC, Mattingly CJ. Comparative Toxicogenomics Database (CTD): update 2021. Nucleic Acids Res. 2021;49(D1):D1138–43.
22. Szklarczyk D, Gable AL, Lyon D, Junge A, Wyder S, Huerta-Cepas J, Simonovic M, Doncheva NT, Morris JH, Bork P, Jensen LJ, Mering CV. STRING v11: protein-protein association networks with increased coverage, supporting functional discovery in genome-wide experimental datasets. Nucleic Acids Res. 2019;47(D1):D607–13.
23. Zhou Y, Zhou B, Pache L, Chang M, Khodabakhshi AH, Tanaseichuk O, Benner C, Chanda SK. Metascape provides a biologist-oriented resource for the analysis of systems-level datasets. Nat Commun. 2019;10(1):1523.
24. Zhu TB, Zhang Z, Luo P, Wang SS, Peng Y, Chu SF, Chen NH. Lipid metabolism in Alzheimer's disease. Brain Res Bull. 2019;144:68–74.
25. Kao YC, Ho PC, Tu YK, Jou IM, Tsai KJ. Lipids and Alzheimer's Disease. Int J Mol Sci. 2020;21(4):1505.
26. Marwarha G, Ghribi O. Does the oxysterol 27-hydroxycholesterol underlie Alzheimer's disease-Parkinson's disease overlap? Exp Gerontol. 2015;68:13–8.
27. Bjorkhem I, Cedazo-Minguez A, Leoni V, Meaney S. Oxysterols and neurodegenerative diseases. Mol Aspects Med. 2009;30(3):171–9.
28. Phan HT, Hata T, Morita M, Yoda T, Hamada T, Vestergaard MC, Takagi M. The effect of oxysterols on the interaction of Alzheimer's amyloid beta with model membranes. Biochim Biophys Acta. 2013;1828(11):2487–95.
29. Park SH, Kim JH, Choi KH, Jang YJ, Bae SS, Choi BT, Shin HK. Hypercholesterolemia accelerates amyloid beta-induced cognitive deficits. Int J Mol Med. 2013;31(3):577–82.
30. Song XY, Zhang TZ, Xu W, He GW, Yan YL. Clinical Observation of Treating Dyslipidemia Accumulation of Phlegm Stasis with Danggui Shaoyao San. J Hebei Tradit Chin Med Pharmacol. 2009;24(01):12–13+2.
31. Fu X, Wang Q, Wang Z, Kuang H, Jiang P. Danggui-Shaoyao-San: New Hope for Alzheimer's Disease. Aging Dis. 2016;7(4):502–13.
32. Dong PL, Zhang TY, Yin X, Wen H, Qu N, Han H. Effect of Danggui Shaoyao Powder on Experimental Hyperlipidemia Model Rats (II). Acta Chinese Med Pharmacol. 2014;42(04):102–4.
33. Popa C, Netea MG, van Riel PL, van der Meer JW, Stalenhoef AF. The role of TNF-alpha in chronic inflammatory conditions, intermediary metabolism, and cardiovascular risk. J Lipid Res. 2007;48(4):751–62.
34. Lehrskov LL, Christensen RH. The role of interleukin-6 in glucose homeostasis and lipid metabolism. Semin Immunopathol. 2019;41(4):491–9.
35. Fatjo-Vilas M, Soler J, Ibanez MI, Moya-Higueras J, Ortet G, Guardiola-Ripoll M, Fananas L, Arias B. The effect of the AKT1 gene and cannabis use on cognitive performance in healthy subjects. J Psychopharmacol. 2020;34(9):990–8.
36. Jayaswamy PK, Vijaykrishnaraj M, Patil P, Alexander LM, Kellarai A, Shetty P. Implicative role of epidermal growth factor receptor and its associated signaling partners in the pathogenesis of Alzheimer's disease. Ageing Res Rev. 2023;83:101791.
37. Marwarha G, Dasari B, Prasanthi JR, Schommer J, Ghribi O. Leptin reduces the accumulation of Abeta and phosphorylated tau induced by 27-hydroxycholesterol in rabbit organotypic slices. J Alzheimers Dis. 2010;19(3):1007–19.
38. Wang T, Feng W, Ju M, Yu H, Guo Z, Sun X, Yang K, Liu M, Xiao R. 27-hydroxycholesterol causes cognitive deficits by disturbing Th17/Treg balance and the related immune responses in mild cognitive impairment patients and C57BL/6J mice. J Neuroinflammation. 2023;20(1):305.
39. Wang Y, Hao L, Wang T, Liu W, Wang L, Ju M, Feng W, Xiao R. 27-Hydroxycholesterol-Induced Dysregulation of Cholesterol Metabolism Impairs Learning and Memory Ability in ApoE epsilon4 Transgenic Mice. Int J Mol Sci. 2022;23(19):11639.
40. Ma WW, Li CQ, Zhao L, Wang YS, Xiao R. NF-kappaB-mediated inflammatory damage is differentially affected in SH-SY5Y and C6 cells treated with 27-hydroxycholesterol. Food Sci Nutr. 2019;7(5):1685–94.
41. Ma WW, Li CQ, Yu HL, Zhang DD, Xi YD, Han J, Liu QR, Xiao R. The oxysterol 27-hydroxycholesterol increases oxidative stress and regulate Nrf2 signaling pathway in astrocyte cells. Neurochem Res. 2015;40(4):758–66.
42. Heverin M, Maioli S, Pham T, Mateos L, Camporesi E, Ali Z, Winblad B, Cedazo-Minguez A, Bjorkhem I. 27-hydroxycholesterol mediates negative effects of dietary cholesterol on cognition in mice. Behav Brain Res. 2015;278:356–9.
43. Ismail MA, Mateos L, Maioli S, Merino-Serrais P, Ali Z, Lodeiro M, Westman E, Leitersdorf E, Gulyas B, Olof-Wahlund L, Winblad B, Savitcheva I, Bjorkhem I, Cedazo-Minguez A. 27-Hydroxycholesterol impairs neuronal glucose uptake through an IRAP/GLUT4 system dysregulation. J Exp Med. 2017;214(3):699–717.
44. Wu M, Zhai Y, Liang X, Chen W, Lin R, Ma L, Huang Y, Zhao D, Liang Y, Zhao W, Fang J, Fang S, Chen Y, Wang Q, Li W. Connecting the Dots Between Hypercholesterolemia and Alzheimer's Disease: A Potential Mechanism Based on 27-Hydroxycholesterol. Front Neurosci. 2022;16:842814.
45. Bjorkhem I. Crossing the barrier: oxysterols as cholesterol transporters and metabolic modulators in the brain. J Intern Med. 2006;260(6):493–508.
46. Testa G, Staurenghi E, Zerbinati C, Gargiulo S, Iuliano L, Giaccone G, Fanto F, Poli G, Leonarduzzi G, Gamba P. Changes in brain oxysterols at different stages of Alzheimer's disease: Their involvement in neuroinflammation. Redox Biol. 2016;10:24–33.
47. Vejux A, Malvitte L, Lizard G. Side effects of oxysterols: cytotoxicity, oxidation, inflammation, and phospholipidosis. Braz J Med Biol Res. 2008;41(7):545–56.
48. Jahn T, Clark C, Kerksiek A, Lewczuk P, Lutjohann D, Popp J. Cholesterol metabolites and plant sterols in cerebrospinal fluid are associated with

Alzheimer's cerebral pathology and clinical disease progression. J Steroid Biochem Mol Biol. 2021;205:105785.
49. Wang HL, Wang YY, Liu XG, Kuo SH, Liu N, Song QY, Wang MW. Cholesterol, 24-Hydroxycholesterol, and 27-Hydroxycholesterol as Surrogate Biomarkers in Cerebrospinal Fluid in Mild Cognitive Impairment and Alzheimer's Disease: A Meta-Analysis. J Alzheimers Dis. 2016;51(1):45–55.
50. Gaschler MM, Stockwell BR. Lipid peroxidation in cell death. Biochem Biophys Res Commun. 2017;482(3):419–25.
51. Rao YL, Ganaraja B, Marathe A, Manjrekar PA, Joy T, Ullal S, Pai MM, Murlimanju BV. Comparison of malondialdehyde levels and superoxide dismutase activity in resveratrol and resveratrol/donepezil combination treatment groups in Alzheimer's disease induced rat model. 3 Biotech. 2021;11(7):329.
52. Esterbauer H. Cytotoxicity and genotoxicity of lipid-oxidation products. Am J Clin Nutr. 1993;57(5 Suppl):779S-785S; discussion 785S-786S.
53. Freeman LR, Keller JN. Oxidative stress and cerebral endothelial cells: regulation of the blood-brain-barrier and antioxidant based interventions. Biochim Biophys Acta. 2012;1822(5):822–9.
54. Liu Z, Liu Y, Tu X, Shen H, Qiu H, Chen H, He J. High Serum Levels of Malondialdehyde and 8-OHdG are both Associated with Early Cognitive Impairment in Patients with Acute Ischaemic Stroke. Sci Rep. 2017;7(1):9493.
55. Dumont M, Beal MF. Neuroprotective strategies involving ROS in Alzheimer disease. Free Radic Biol Med. 2011;51(5):1014–26.
56. Ito F, Sono Y, Ito T. Measurement and Clinical Significance of Lipid Peroxidation as a Biomarker of Oxidative Stress: Oxidative Stress in Diabetes, Atherosclerosis, and Chronic Inflammation. Antioxidants (Basel). 2019;8(3):72.
57. Ayala A, Munoz MF, Arguelles S. Lipid peroxidation: production, metabolism, and signaling mechanisms of malondialdehyde and 4-hydroxy-2-nonenal. Oxid Med Cell Longev. 2014;2014:360438.
58. Chen JJ, Thiyagarajah M, Song J, Chen C, Herrmann N, Gallagher D, Rapoport MJ, Black SE, Ramirez J, Andreazza AC, Oh P, Marzolini S, Graham SJ, Lanctot KL. Altered central and blood glutathione in Alzheimer's disease and mild cognitive impairment: a meta-analysis. Alzheimers Res Ther. 2022;14(1):23.
59. Biswas SK. Does the Interdependence between Oxidative Stress and Inflammation Explain the Antioxidant Paradox? Oxid Med Cell Longev. 2016;2016:5698931.
60. Leng F, Edison P. Neuroinflammation and microglial activation in Alzheimer disease: where do we go from here? Nat Rev Neurol. 2021;17(3):157–72.
61. Lyman M, Lloyd DG, Ji X, Vizcaychipi MP, Ma D. Neuroinflammation: the role and consequences. Neurosci Res. 2014;79:1–12.
62. Griffin R, Nally R, Nolan Y, Mccartney Y, Linden J, Lynch MA. The age-related attenuation in long-term potentiation is associated with microglial activation. J Neurochem. 2006;99(4):1263–72.
63. Cai Z, Hussain MD, Yan LJ. Microglia, neuroinflammation, and beta-amyloid protein in Alzheimer's disease. Int J Neurosci. 2014;124(5):307–21.
64. Y Niu, SF Wang. Analysis on chemical constituents in Danggui-Shaoyao-San by LC-Q-TOF-MS and LC-IT-MSn. Chinese Traditional and Herbal Drugs. 2014;45(08):1056-1062.
65. X Liu, ZP Sun, KM Qin, JJ Jin, C Yang, BC Cai. To study the effect of processing on the chemical components of Atractyloides Shaoyao powder based on UHPLC-Q-TOF-MS technolog. Chinese Traditional and Herbal Drugs. 2022;53(13):3920-3928.
66. K Pei, Y Ning, H Cai. Mechanism Analysis of Strengthening Anti-cerebral Ischemia Injury of Chuanxiong Rhizoma Processed with Wine Based on UHPLC-Q-Orbitrap HRMS and Integrated Network Pharmacology. Chinese Journal of Experimental Traditional Medical Formulae. 2022;28(12):164-173.
67. X Gao, WJ Sun, L Qi, Y Li. Ultra-performance liquid chromatography coupled with electrosprayionization/quadrupole time-offlight mass spectrometry for the rapid analysis of constituents in Chuanxiong Rhizoma. Northwest Pharmaceutical Journal. 2018;33(06):711-715.
68. X Sun, HM Wen, XB Cui, TL Lu, W Li, CX Shan. Qualitative evaluation of Atractylodis Macrocephalae Rhizoma from different habitats by HPLC-PDA fingerprint combined with UFLC-Q-TOF/MS qualitative identification. Chinese Traditional and Herbal Drugs. 2016;47(19):3494-3501.
69. J He, XX Gao, JS Tian, XM Qin, GH Du, YZ Zhou. Changes of chemical composition of Bupleuri Radix-Paeoniae Radix Alba herb pair before and after compatibility by UPLC-MS background subtraction and metabonomics-sHE. Chinese Traditional and Herbal Drugs. 2018;49(08):1779-1788.
70. X Lin, WX Li, JY Wang, Y Zhao, YJ Cao. Analysis of Chemical Constituents of Shaoyao Decoction by UPLC-Q-TOF-MS. Modern Chinese Medicine. 2021;23(01):48-56.
71. YY Luo, XW Qian, XX Shha. Analysis of Chemical Constituents of Atractylodes macrocephala Koidz. Processed by Different Drying Methods by UPLC-QTOF MS with Multivariate Stastistical Analysis. Chinese Pharmaceutical Journal. 2022;57(10):784-790.
72. Y Song, LH Sheng, LS Sheng, P Li. Analysis of the Composition in Danggui Buxue Decoction by LC-ESI/TOF MS. Chinese Journal of Natural Medicines. 2005(05):298-302.
73. ZM Yao, WD Chen, ZH Yang. Research progress in Atractylodes macrocephala and predictive analysis on Q-marker. Chinese Traditional and Herbal Drugs. 2019;50(19):4796-4807.
74. YM Zhong, YF Feng, J Guo. Rapid Identification of Components fromAtractylodis macrocephalae Rhizoma Based on UPLC/Q-TOF MS. Journal of Chinese Mass Spectrometry Society. 2015;36(01):72-77.
75. Q Xiang, WY Zhao, C Wang. Analysis of Terpenoids in Alismatis Rhizoma Before and After Processing with Salt-water Based on UPLC-Q-TOF-MS. Chinese Journal of Experimental Traditional Medical Formulae. 2022;28(19):154-161.
76. Y Liu, YP Yang, BB Shen. Chemical constituents of Fangji Fuling decoction by HPLC-Q-TOF-MS/MS. Central South Pharmacy. 2021;19(08):1563-1569.

Publisher's Note